



Evaluation of a liquid crystal based polarization modulator for a space mission thermal environment



Manuel Silva-López^{a,*}, Laurent Bastide^a, René Restrepo^b, Pilar García Parejo^a,
Alberto Álvarez-Herrero^a

^a Instituto Nacional de Técnica Aeroespacial (INTA), Área de Instrumentación Óptica Espacial, Carretera de Ajalvir, Km. 4, Torrejón de Ardoz, 28850 Madrid, Spain

^b Applied Optics Group, Universidad EAFIT, Carrera 49# 7, Sur-50, Medellín, Colombia

ARTICLE INFO

Article history:

Received 26 April 2017

Received in revised form

18 September 2017

Accepted 19 September 2017

Available online 21 September 2017

MSC:

00-01

99-00

Keywords:

Liquid crystal

Thermal analysis

Wavefront measurement

Interferometry

Optical metrology

Space mission

ABSTRACT

The Multi Element Telescope for Imaging and Spectroscopy (METIS) is one of the remote sensing instruments to be onboard the future NASA/ESA Solar Orbiter mission. The science nominal mission orbit will take the spacecraft from 0.28 to 0.95 astronomical units from the Sun, setting challenging and variable thermal conditions to its payload. METIS is an inverted-occultation coronagraph that will image the solar corona in the visible and UV wavelength range. In the visible light path a Polarization Modulation Package (PMP) performs a polarimetric analysis of the incoming solar light. This PMP is based on liquid crystal variable retarders (LCVR) and works under a temporal modulation scheme. The LCVRs behavior has a dependence on temperature and, as a consequence, it is critical to guarantee the PMP performance in the mission thermal environment. Key system specifications are the optical quality and the optical retardance homogeneity. Moreover, the thermally induced elastic deformations of the mechanical mounts and the LCVRs shall not produce any performance degradation. A suitable thermal control is hence required to maintain the system within its allowed limits at any time. The PMP shall also be able to reach specific set-points with the power budget allocated. Consequently, and in order to verify the PMP thermal design, we have experimentally reproduced the expected thermal flight environment. Specifically, a thermal-vacuum cycle test campaign is run at the different mission operational conditions. The purpose is both to check the stability of the thermal conditions and to study the optical quality evolution/degradation. Within this test transmitted wavefront measurements and functional verification tests have been carried out. To do that we adapted an optical interrogation scheme, based on a phase shifting interferometric technique, that allows for inspection of the PMP optical aperture. Finally, measurements obtained at non-operational temperature conditions are also shown. These results demonstrate that the device meets the specifications required to perform its operational role in the space mission environment.

© 2017 The Authors. Published by Elsevier B.V. This is an open access article under the CC BY-NC-ND license (<http://creativecommons.org/licenses/by-nc-nd/4.0/>).

1. Introduction

The future Solar Orbiter (SolO) ESA/NASA mission is intended to perform measurements of the inner heliosphere, nascent solar wind, and close observations of the polar regions of the Sun [1]. The spacecraft (S/C) is a Sun-pointed, 3-axis stabilized platform, with a dedicated heat shield to provide protection from the high levels of solar flux near perihelion. Its payload suite combines remote sensing with in situ analysis instrumentation. Suitable fields-of-

view to the Sun are provided for the remote-sensing instruments by means of feedthroughs in the heat shield.

The challenging orbit of the mission imposes harsh thermal environments on all on board subsystems. During the science mission the S/C distance to the Sun will oscillate between 0.28 and 0.95 astronomical units (AU) in about 3 months time, thus exposing the platform to very different irradiation conditions. As a consequence, and for a suitable optical performance, a careful thermal modeling and a thorough experimental validation of the instruments in their thermal flight environment is required.

One of the remote sensing instruments on board SolO is the Multi Element Telescope for Imaging and Spectroscopy (METIS) [2]. METIS is an externally occulted coronagraph. This instrument uses a polarimeter to analyse the visible components of the coronal light.

* Corresponding author.

E-mail address: silvalm@inta.es (M. Silva-López).

A section of this polarimeter is a Polarization Modulator Package (PMP) designed to perform temporal modulation of the incoming light [3].

The PMP is based on Liquid Crystal Variable Retarders (LCVRs). Our team have performed an extensive validation campaign of LCVRs for aerospace applications [4,5]. Among other tests, we have evaluated the impact of vacuum, temperature and radiation on the optical performance, such as optical retardance or response time. Our work led to the development of the successful IMAx instrument, a LCVR based spectro-polarimeter, on board the stratospheric Sunrise I and II missions [6,7]. These were projects within the NASA Long Duration Balloon Program. As a consequence of this work LCVRs will be used not only in the METIS PMP, but also in other two modulators within the Polarimetric and Helioseismic Imager, another remote sensing instrument on board SoHO [8,9].

Moreover, although LCVRs is a well-known technology for ground applications in astronomy [10,11], this is, to our knowledge, the first time it will be used in a space instrument. LCVRs become a powerful alternative to the traditional rotating polarizing optics since they require less mass, volume and do not need to use any form of mechanisms [12]. The LCVRs response times are in the range of tens of milliseconds or better, adequate for a space spectro-polarimeter. They are also easy to synchronize with the detector readout, due to their electro-optical nature, thus simplifying instrument control. These are significant advantages for an instrument on board a spacecraft, where the resources are very limited and the risk of a mechanical failure must be minimized.

In the first sections of this paper the METIS PMP and its main thermal-related requirements are described. A key constraint for the PMP design is the thermal stability required during the polarimetric measurements. As a consequence, specific temperature set-points are defined within its operational temperature range. These set-points can be selected as a function of the flight environment. Then, an experimental arrangement to set this environment is presented and a thermal analysis verifies the suitability of this arrangement.

The second half of this work deals with the PMP thermo-vacuum test campaign. The device is subjected to the mission operational conditions in a thermal cycle test using the experimental arrangement previously described. The thermal control is programmed to establish the different set-points along these cycles. The main objective here is to verify the PMP thermal control in the expected mission environment. Combined to this test we perform optical quality measurements of the PMP optical aperture in order to check that the thermo-elastic deformation of the components (i.e. LCVRs, mechanical mounts, ...) do not produce any degradation. This is done by means of a phase shifting interferometric technique, that we have adapted to our set-up. Thus, transmitted wavefront measurements were obtained in order to verify the performance and degradation of the device. In addition, functional verification of the LCVRs was also performed during this thermo-vacuum test.

Finally, a list of other parameters, evaluated at the non-operational temperatures, are given in the last section. However, it is important to mention that the tests described here are just a fraction of the complete acceptance campaign at the subsystem level. These tests are preceded and followed by other tests such as radiation, vibration and more specific tests, such as the characterization of the polarimetric efficiencies, following the method described in the literature [4,13].

2. The Multi Element Telescope for Imaging and Spectroscopy

METIS consists of a coronagraph for the study and characterization of the solar corona. METIS is based on a novel design, which

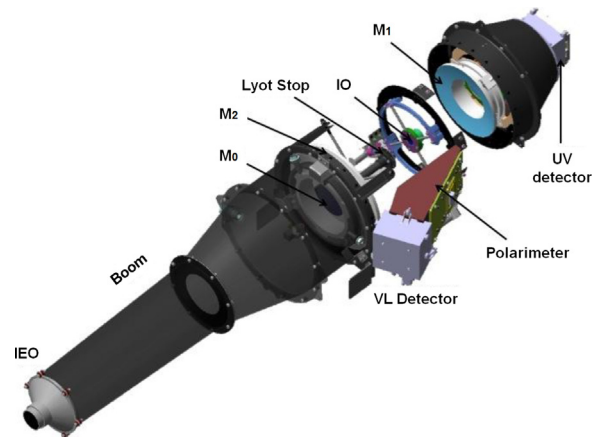


Fig. 1. METIS optomechanical layout showing the main telescope elements. The PMP is a section of the polarimeter.

introduces the concept of occulter inversion in solar coronagraphy [2]: the coronal light enters through a circular aperture ($\varnothing 40$ mm) acting as an Inverted External Occulter (IEO) located on the outside panel of the heat shield. The IEO is supported by a suitable truss (boom) which protrudes from the S/C instrument bay through the heat shield. Fig. 1 shows a CAD model of the instrument.

A $\varnothing 71$ mm spherical mirror (M_0) rejects back the disk light through the IEO up to 1.1° , this is 1.17 times the apparent solar radii at a distance of 0.28 AU. The coronal light is collected by an on-axis Gregorian telescope. The suppression of the diffracted light off the edges of the IEO and M_0 is achieved by, respectively, an Internal Occulter (IO) and a Lyot trap.

The METIS optical configuration includes visible light (VL) and UV imaging. Moreover, the inverted occultation concept can also accommodate a EUV spectrograph maintaining the same basic optical layout. The design of this coronagraph minimizes the solar flux entering the instrument [14].

The METIS polarimeter arm includes a number of polarization optics in a Senarmont configuration [15]. After diffraction in M_1 , visible light is transmitted by a bandpass filter (580–640 nm). The optical path travels through a fixed quarter-wave retarder (at 0° with respect to the PMP LCVRs fast axis), the PMP itself, and a linear polarizer (analyzer with transmission axis at 45°) before reaching the VL detector.

Consequently, the METIS polarimetric system will measure the Q and U Stokes parameters corresponding to the linear polarization components of the incoming solar light. The polarization modulation shall be carried out by the PMP, which generates different modulations of the polarization state by controlled changes in the optical retardance.

3. The Polarization Modulation Package

A partially exploded view of the PMP is shown in Fig. 2(a). The PMP main structure is manufactured of titanium (Grade 5) in order to have enough mechanical stiffness, withstand high mechanical loads and provide for thermal insulation. It is finished with an Astroblack coating (Metal Estalki S.L.) to fulfill the straylight requirements. The PMP consist of two identical LCVR assemblies. Each assembly allocates one LCVR, its aluminum mounting rings, a heater and a thermal sensor. Fig. 2(b) shows a picture of the PMP flight model.

The driving voltage is applied to the LCVRs through a kapton flexible cable attached to the cells using an electrical conductor glue (Eccobond 56C, Henkel). The kapton cable also includes the signal of the Pt100 temperature sensor (model POTL1102, Rose-

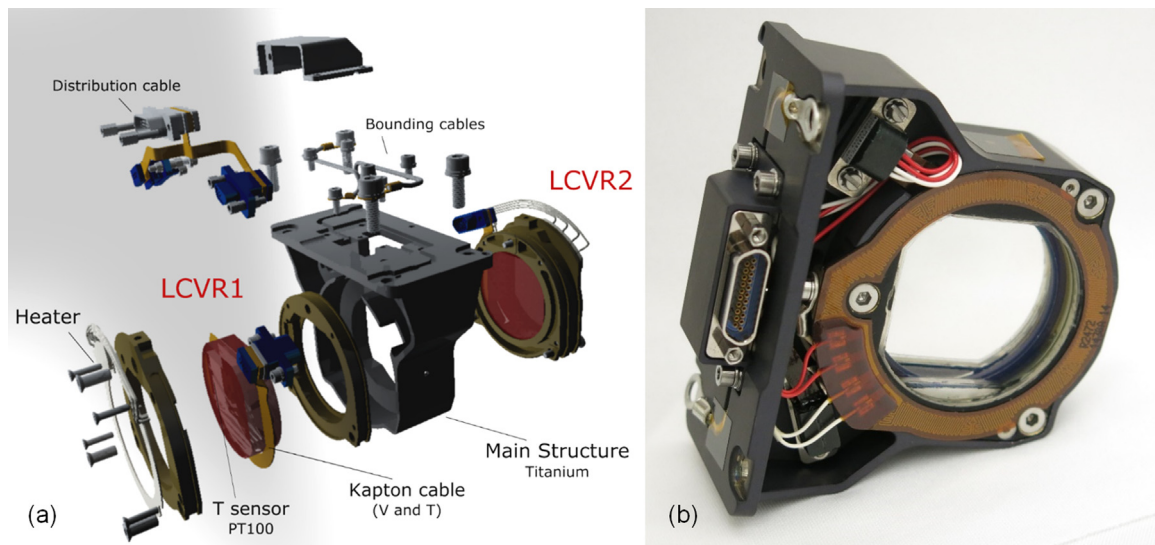


Fig. 2. (a) Partially exploded-view drawing of the METIS PMP. The two LCVR assemblies are the main components. (b) Picture of the PMP flight model.

mount Aerospace). These sensors are used for the active thermal control of the LC (liquid crystal) cell. To improve thermal contact the cells are mounted into two aluminum rings. These rings have a circular polyimide heater attached that can provide a maximum of 4 W of heating power. All the electrical signals are connected to the electrical unit of the instrument through the distribution cable.

The mounting aluminum rings (AL 6082-T651) are black anodized [16] and have been designed to minimize thermo-elastic deformations produced during thermal cycling. A silicone material (MAPSIL QS 1123) is applied between the opto-mechanical mount and the LC cells that will serve as the elastic material to protect the cells from the vibration and shock loads. Overall the opto-mechanical mount ensures that no stressing loads are applied to the LCVRs in order to avoid induced birefringence and wavefront distortion.

Coronagraphs are instruments characterized by having a wide field-of-view. Specifically, the METIS PMP will have to work with collimated rays and angles of incidence up to $\pm 7^\circ$. Polarization optics, in particular retarders, are sensitive to the angle of incidence as their optical retardance changes with the incident angle. For this reason, a double-cell configuration was chosen. The PMP is thus formed by two identical APAN (Anti-Parallel Aligned Nematic) cells stacked together and with their LC molecules tilted in opposite directions. The LCVR are oriented with their fast axis parallel to each other. This system yields a polarization modulator with lower angular dependence and therefore higher incident acceptance angle [17].

The LCVR cell design consists of two glass substrates of 5 mm thickness, coated on one side with Indium Tin Oxide (ITO) and on the other side with an antireflective coating. The LCVR details are described in the literature [8]. The cell is assembled together and partially sealed to let an opening for LC filling. Finally the cell is completely sealed with an UV cured glue or stopper and an external part of the ITO coating is electrically connected to the electrode.

The PMP has been designed not only to reduce the mechanical stress produced by the mounts to the cells, but to minimize mass, volume and thermal inhomogeneities. It has also been considered the vibration environment, due to the launch loads, that the device shall withstand. Finally, the electrical cables and connections are arranged to obtain a compact, modular and robust device.

Table 1

A partial PMP subsystem requirement list.

Parameter	Specification
Working wavelength	580–640 nm
Optical quality	<100 nm WFE rms
Clear aperture	>ø30 mm
Non-operational temperature range	[−40 °C, 90 °C]
Operational temperature range	[−20 °C, 85 °C]
Science set-points	[30 °C, 50 °C, 70 °C]
Temperature homogeneity on LCVRs	±1 °C
LCVR response time	<1 s
Power consumption (heaters)	≤4 W
Testing pressure	≤1.3 mPa

3.1. Requirements and constraints driving the design

The METIS thermal control system has the objective of maintaining the critical components within specific temperature ranges with the maximum efficiency and minimum resources. Some of its design drivers are the following: Maintain the optical performance of the instrument at all times by eliminating temperature gradients on optical components; insulate METIS from parasitic heat loads from other S/C instruments, dispose off the undesired infrared radiation from the feedthroughs or interfaces and an improved stray light suppression [14].

The METIS anti-reflecting coating is optimized for the working wavelength, which is the range 580–640 nm. The optical quality of the PMP shall be <100 nm rms for the wavefront error (WFE) at the operational wavelength, and this includes mounting effects (i.e. thermoelastic deformations) at operational conditions. This requirements are listed in Table 1.

Table 1 also shows some of the PMP specifications driven by the thermal control requirements. They are given by the specific SolO mission characteristics. The mission orbit will oscillate from 0.28 to 0.95 AU in about 3 months time. This sets the non-operational temperature range to have a 130 °C variation. This corresponds to a $\sim 1.5^\circ\text{C}$ change per day during the mission cruise phase. However this variation can reach $\sim 5^\circ\text{C}$ per day around perihelion.

Key requirements are given by the fact that LCVRs have a dependence on temperature: molecular order is affected by thermal agitation. Consequently, thermal control must be considered in order to obtain a suitable repeatability of the optical retardance induced. In particular, to obtain a response time suitable for the

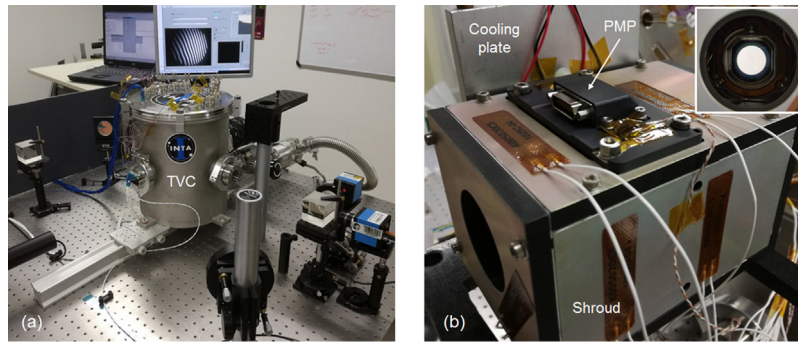


Fig. 3. (a) Overall view of the optical setup. The TVC, on top of an optical rail, is placed in the measurement path of a Mach–Zehnder interferometer. (b) Thermal shroud with the PMP inserted and the thermoelectric components attached. Two Peltier elements, not visible in the image, are placed in between the shroud and the cooling plate. The thermofoil heaters are seen in three of the visible faces. The inset shows the PMP clear aperture through the shroud holes.

Table 2
Set-point system temperatures.

Set-point	1	2	3
PMP LCVR cell	30 °C	50 °C	70 °C
PMP BP	–20 °C	30 °C	50 °C

acquisition process, that is <1 s, and to simplify calibration processes, the LCVRs shall work from 30 °C.

The METIS thermal control shall maintain the temperature of the PMP stable at specific science set-points. These set-points are defined so that the PMP temperature is always above the environment. A representative reference point of the thermal environment is the temperature at the PMP baseplate (BP). Depending on this environment the three selectable set-points are shown in Table 2.

To reach these conditions a temperature controller, located in the METIS Electronic Unit, is used to manage the power supplied by the heaters. This power will depend on the LCVR temperature (monitored by the Pt100 sensors) and the set-points defined in the software. Nevertheless, and this is another requirement, the maximum allocated power to heat up the PMP is 4 W (provided by a 28 V supply). In this regard the most restrictive condition, the set-point 1 with a 50 °C thermal gradient, shall be ensured by thermal control.

Finally, and to fulfill the required polarimetric accuracy the temperature homogeneity across the PMP clear aperture shall be better than ± 1 °C. It is clear that careful thermal design is key to obtain the thermal stability required for the polarimetric measurements.

4. Thermal characterization

In this section the experimental arrangement employed during the thermal cycling test is described. The experimental setup and all the thermo-electric components required to set the representative environment are listed. Alternatively, a thermal modelling software was used to model the system and calculate the power required to set the target conditions.

4.1. Test assembly

To simulate the space environment a thermal vacuum chamber (TVC) was used. The TVC, shown in Fig. 3(a), has a cylinder shape with 26 cm of inner diameter and 28 cm height. It provides feedthroughs for connections to all the thermo-electric elements and the PMP. The chamber has two opposite located optical windows that allow optical interrogation of samples. Finally, a primary pump and a turbomolecular pump (Varian, Turbo-V 81-M) connected to the chamber sets the vacuum levels required for the tests.

To set the thermal environment a shroud was placed inside the TVC. This thermal shroud is a 79 mm × 90 mm × 130 mm aluminum (Al 6082) box with a 7 mm thick wall designed to match the polarimeter section where the PMP is allocated. Cho-Therm (Chomerics) interfiller is used to improve the thermal contact between each face of the shroud. Fig. 3(b) shows a picture of the system ready to be placed inside the TVC. Circular holes (30 mmØ) at opposite walls allow for optical inspection across the clear aperture of the PMP. Moreover, a black anodizing process [16] was applied in the inner walls of the box to reproduce the METIS thermal finish, which uses black anodized to avoid straylight effects. Finally, and in order to help thermal control and to limit heat losses by radiation, the outer walls of the box were alodined (Alodine 1200S) and a single insulating layer (aluminized Mylar) was placed above this thermal shroud.

To set the hot case conditions thermofoil heaters (K005020C5, Watlow) are attached to the walls of the shroud. These are nine Polyimide film heaters (160 Ω and 51 mm × 13 mm size per unit), attached to the six faces of the shroud. Considering the heaters maximum rated power (2.9 W) we can provide 26 W to the shroud.

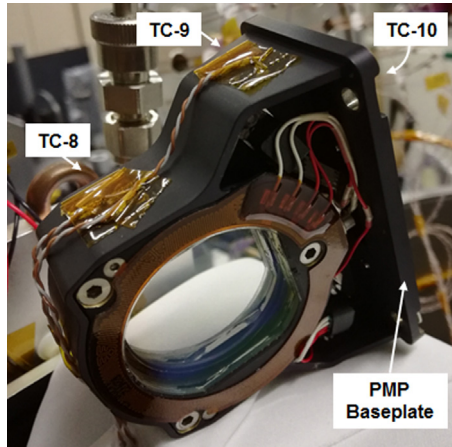
To cool down this shroud a couple of 30 mm × 30 mm Peltier elements (model ETH-127-10-13-RS, Adaptive), connected in parallel, are attached between one of the walls of the shroud and the cooling plate, which is used as a heat sink by the Peltier elements. Each element has a maximum cooling capacity of 37.9 W (with 3.9 A) and a 0.2 mm thick interfiller is used on both sides to improve thermal contact. The hot side of the Peltier elements is in contact with a cooling plate as shown in Fig. 3(b). This plate includes an internal pipe where a liquid coolant (water plus ethylene-glycol) flows through. This circuit is connected to a refrigeration unit (Grant R1) that enables a thermal stabilization in the range –20 °C to 30 °C. The most critical situation is the set-point 1, as shown in Table 2, with a 50 °C temperature difference between the cell and the environment. Experimentally, this must be achieved by both warming up the PMP heaters and cooling down the environment.

Table 3 shows a list of the sensors used for housekeeping (HK), control and monitoring of the thermal conditions during the tests. Type T thermocouples (TC) were attached to the PMP, shroud, cooling plate and TVC. The PID control units are used to establish the set-points thermal conditions according to Table 2. One of the internal PMP sensor, the Pt100 from the LCVR₁, is used as a temperature reference point (TRP) for monitoring purposes. The other Pt100 is employed by the PID thermal control unit. A data acquisition unit (Fluke NetDaQ 2640A) connected to a computer is used as a data logger with a sampling time of 2 min.

Five TC are used to monitor the radiative interface (IF) environment of the PMP (the inner faces of the shroud). Moreover, three TC are dedicated to the PMP structure, as it is shown in Fig. 4 (and in Fig. 3(b)). TC-8 and TC-9 are attached to one side and TC-10 mon-

Table 3
Temperature sensors.

	Position	Type	Function
1	PMP cell 1	Pt 100	Monitoring (TRP)
2	PMP cell 2	Pt 100	PMP thermal control
3	PMP radiative IF (top)	TC	HK
4	PMP radiative IF (cooling plate side)	TC	HK
5	PMP radiative IF (opposite cooling plate)	TC	HK
6	PMP radiative IF (lateral)	TC	HK
7	PMP radiative IF (bottom)	TC	Shroud thermal control
8	PMP structure	TC	HK
9	PMP structure	TC	HK
10	PMP structure (baseplate)	TC	Monitoring
11	Cooling plate	TC	HK
12	TVC	TC	HK

**Fig. 4.** Location of the thermocouples on the PMP structure.**Table 4**
Number of nodes and surface optical properties of the thermal mathematical models.

Element	Nodes	IR emissivity
TVC	72	0.4
Cooling plate	1	0.4
PMP shroud	76	Outside (Alodine 1200S): 0.15 Inside (Black anodized): 0.85
PMP	34	Titanium structure: 0.9 LCVR cell: 0.9 Ring polyimide heater: 0.85

itors the PMP baseplate temperature. This baseplate is in direct contact with the top radiative and conductive IF (top face of the shroud). This baseplate temperature and the TRP are used to infer the PMP thermal gradient.

4.2. Thermal mathematical model and analysis

To set the flight conditions expected during the mission, a thermal simulation of the experimental arrangement was performed. This simulation is mandatory in order to estimate that a representative thermal environment can be set. The extremes of the operational temperature range, according to Table 1, will be evaluated in our simulations.

The Esatan-TMS (ITP Engines UK) thermal modeling suite was used to build the thermal models and run the calculation. These models are the TVC, the cooling plate, the shroud and the PMP. They are shown in Fig. 5(a). Two views of the shroud thermal model with the heater positions in red are shown in Fig. 5(b). To reach a suitable precision in the calculation, each model was meshed as detailed in Table 4. In particular, the geometrical thermal model of the PMP is

composed of 15 shells, 60 active faces and 8 inactive faces with a total of 34 thermal nodes. The radiative couplings inside the TVC were computed by the software using the IR emissivity also detailed in Table 4.

Fig. 6 presents a simulated temperature distribution of the shroud and the PMP in hot and cold conditions. For the hot conditions, illustrated in Fig. 6(a) we calculated that the shroud heaters need to provide 10.2 W to set the shroud temperature in the range of 80–90 °C. This, in turn, sets the PMP optical aperture to 85 °C. Two views of the shroud are shown to illustrate its gradient (mainly due to heat losses by conduction with the cooling plate). All the thermofoil heaters of the experimental arrangement can provide more than double the power estimated in this simulation.

On the other hand, Fig. 6(b) shows a simulated temperature distribution of the thermal models in the cold case. Here we are taking into account that previous experiments have shown that the cooling plate (connected to the refrigeration unit) has a limited capacity to evacuate the heat dissipated by the Peltier elements. Thus, in this simulation, we are considering the Peltier hot side (cooling plate) at 0 °C. In this situation, and in order to set the PMP at –20 °C, it was estimated that each Peltier element requires 0.8 A to cool down the shroud. This current can be supplied, and it is compatible, with the arranged Peltier elements.

Overall these simulations demonstrate that the environment conditions required for the METIS PMP operation can be met by our setup.

5. Transmitted wavefront in situ measurements

Before proceeding with the thermal vacuum test campaign, and to check a basic performance, a number of thermal images were obtained at room conditions using an infrared camera (Thermo Vision A320, Flir Systems). The thermal images, illustrated in Fig. 7, show the PMP from both sides under heater operation and in thermal equilibrium. 20 min were required to reach equilibrium from 20 °C to 40 °C. The LCVR temperature sensors, which are embedded in the aluminium rings on top of the substrates, were stable at 40 °C. The images reveal that the temperature difference from center to side at the clear aperture (ø30 mm) is below 1. They provide a first approximation to the thermal gradient present across the aperture. However the low power applied and the presence of air, and therefore homogenization due to convection, cannot be neglected.

5.1. Optical setup arrangement

The thermal test assembly described in Section 4 is employed in the optical setup arrangement, and a diagram is shown in Fig. 8. In this set up, a light beam from a He-Ne laser source (633 nm) is expanded and collimated. The PMP is placed in the shroud and this, in turn, is placed inside the TVC. The beam that travels through the TVC is later combined with a reference beam to set a Mach–Zehnder interferometer arrangement. Then a fringe pattern is formed and focused into a CCD camera (DFK41BU02.H model, Imaging Source). The camera has a 1280 × 960 pixel array with a 4.65 μm pixel size. Moreover, the TVC is placed in an optical rail so that it can be removed from the interferometer. This is convenient to extract the wavefront distortion produced by the rest of the optics of the set up, as we shall see.

In particular, and to evaluate the refractive index homogeneity of the sample, we perform a transmitted wavefront quality test by means of a phase shifting interferometric technique [15]. The measuring optical path of the interferometer uses a mirror with a piezo motor linear stage (model AG-LS25, Newport) that is used to change the optical path. The sample (PMP) is placed in the optical path of

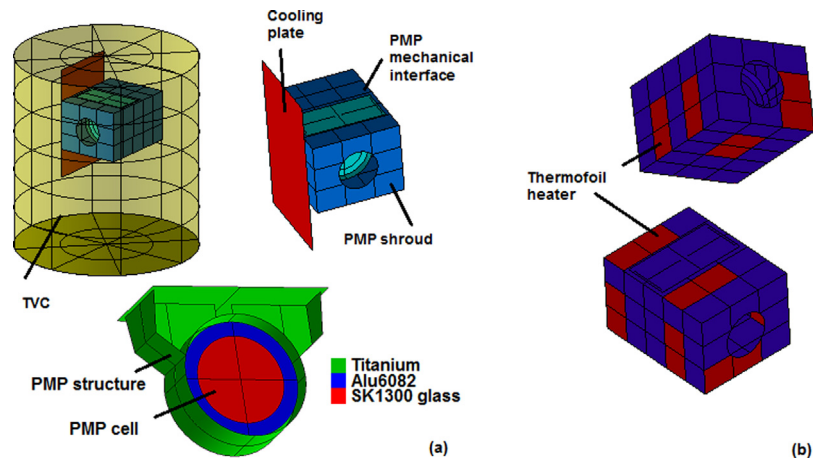


Fig. 5. Mathematical models of the thermal system. (a) Within a cylinder shaped TVC the PMP shroud is placed, this, in turn, is in contact with the cooling plate. Inside the shroud is located the PMP thermal model. (b) The heaters position on the shroud thermal model (from two points of view).

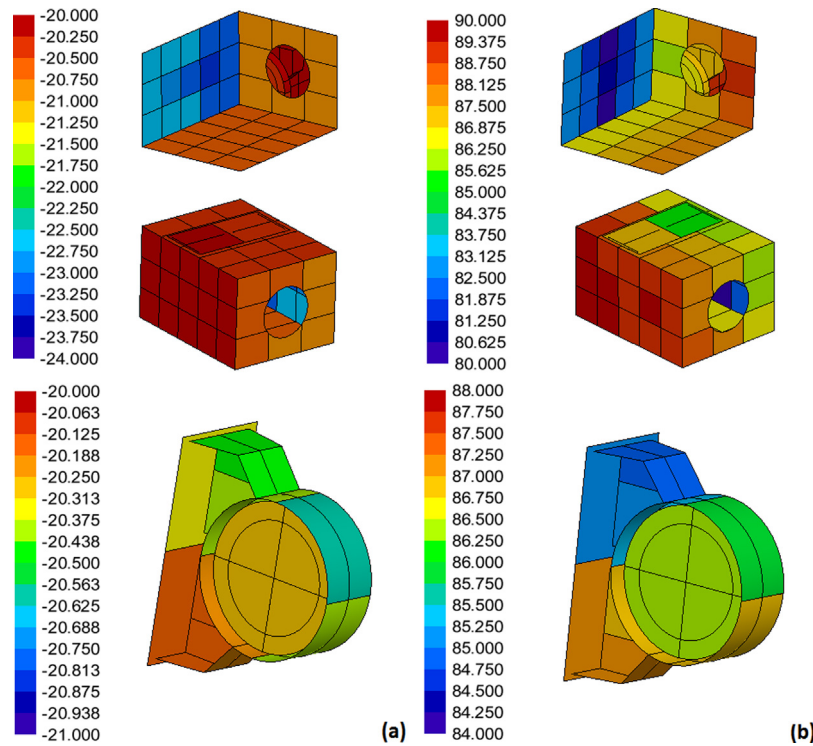


Fig. 6. Estimated shroud and PMP temperature distribution on (a) cold and (b) hot conditions. The PMP clear aperture is at -20°C and 85°C , respectively.

one of the arms of a Mach–Zehnder interferometer, as illustrated in Fig. 8. Thus an interference fringe pattern will be projected on the camera focal plane. The piezo stage and the camera are controlled via LabView (National Instruments). The system obtains interferograms under different phase shifting conditions and calls Matlab for the fringe processing. This processing is based on a least-squares iterative procedure algorithm [18]. The method provides accurate extraction of phase information, even in the presence of vibrations, with as few as three randomly shifted interferograms [19,20]. An example of an interferogram captured can be seen in Fig. 9(a).

5.2. Wavefront quality evaluation

A PMP transmitted wavefront characterization is performed in two steps. First, the phase is recovered using the interferometric set up shown in Fig. 8. This phase measure will be denoted as ϕ_{TVC} .

For the second step the TVC is removed from the set up, leaving the measuring arm of the interferometer unobstructed. The measuring procedure is repeated and the phase obtained is ϕ_{ARM} . Once the phase measurements in both cases are obtained, the wavefront error (WFE) caused by the PMP is computed by subtracting:

$$WFE = \phi_{\text{TVC}} - \phi_{\text{ARM}} \quad (1)$$

The procedure allows us to characterize the retardance homogeneity of the PMP, among other transmission optical devices. Measurements of the WFE will be obtained, using this method, during the thermal cycling campaign.

We cannot, however, remove the influence of the optical windows of the TVC in the WFE measurement. To evaluate this influence we have performed measurements with an empty TVC at vacuum conditions. The WFE obtained is shown in Fig. 9(b). The wavefront is fitted to the first 45 Zernike polynomials, save for the

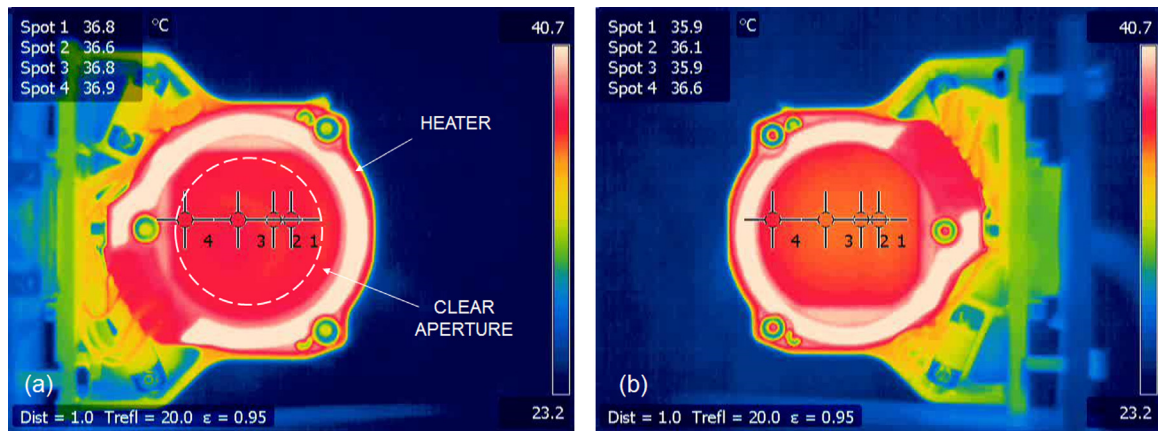


Fig. 7. Thermal images of the PMP obtained by a thermal IR camera. The device was set by action of the heaters at 40 °C at room pressure. (a) Front side of the PMP, showing the first LCVR assembly. The operational clear aperture is marked with a dotted line. (b) Back side of the device. Within the clear aperture the temperature difference was measured to be <1 °C.

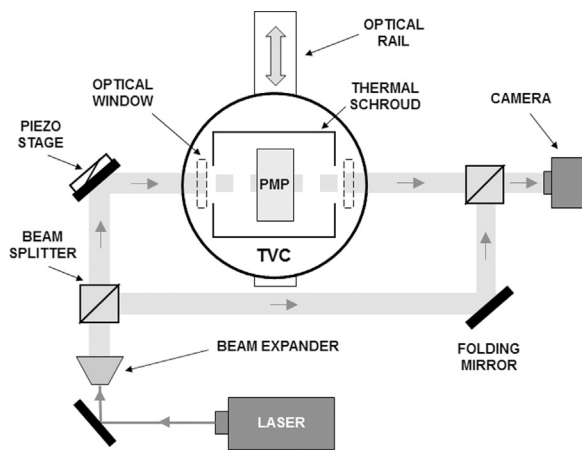


Fig. 8. Diagram of the optical interrogation set up. A thermal vacuum chamber (TVC) with suitable optical windows is set for the optical interrogation in the measuring arm of a Mach-Zehnder interferometer. The TVC can move along an optical rail so that it can be completely removed from the optical path. To induced differential phase shifts a piezo driven stage is attached to a folding mirror.

piston and tilt components. The results show that the chamber windows has an optical flatness in the order of $\lambda/25$ (peak to valley) and with a WFE(rms) < 0.005 λ . As a consequence we will consider this influence negligible.

6. Measurement campaign

The baseline test program consists of four thermal cycles to be performed at qualification level. The thermal cycles cover the operative range, i.e. each cycle oscillates from −20 °C to 85 °C. However, the first and fourth cycle include steps at the science set-points temperatures, and transmitted wavefront measurements are performed at these conditions. For each step a dwell time of 2 h is considered and the stabilization criteria for the TRP is 1 °C per hour. The temperature profiles of the TRP and the PMP baseplate (BP) are shown in Fig. 10, where the transient periods were removed for clarity.

In addition to the PMP set-points, an additional step was included at 40 °C for the TRP, for which we achieved the highest temperature gradient with respect to the BP (52 °C difference). Fig. 11 shows a detail of the fourth thermal cycle, and the thermal readings obtained (sampling time 2 min).

6.1. Transmitted wavefront results

The WFE evolution along the thermal vacuum test is summarized in Fig. 12. The WFE shows a slight astigmatic aberration at 30 °C, as illustrated in the top row. The first and second column shows data from the first and fourth cycle respectively. It is interesting to note that a negative wavefront distortion (at the bottom of each image) corresponds to the region next to the filling inlet of the cells. The cavity is sealed with a glue, which may be partially diffused with the LC molecules. At room temperature, this diametrical diffusion across the clear aperture produces a WFE with a significant vertical astigmatism.

As temperature increases the wavefront changes from cylindric to a spherical aberrated wavefront, as illustrated in the second and third row of Fig. 12. This phenomenon is enhanced as the temperature reaches 85 °C, (fourth row), where the power of the spherical component of the wavefront is increased. This behaviour was found to be elastic, and the same wavefront shape was recovered at each temperature set-point. We believe that the WFE evolution may be due to a thermal induced diametral force. This increasing force may be due to a differential thermal expansion of the cell components as well as a possible contribution from the mounting rings [21].

The subtraction of the wavefront obtained at the same temperature conditions in different cycles is shown in the third column of Fig. 12. The differences are negligible: notice that the scale of the plot was reduced in order to show variations with respect to a flat wavefront. This shows a good repeatable and elastic behaviour.

Low order Zernike modes are typical from stress-induced birefringence, or thermal induced deformations. This is illustrated in Fig. 13. This plot shows the Zernike coefficients obtained from two wavefront measurements at different temperatures. Their main contributions are clearly the defocus and the vertical astigmatism, for the wavefronts obtained at 85 °C and 30 °C, respectively. The next relevant contributions are from spherical and coma aberrations, while the rest of the 45 coefficients are almost negligible.

Two parameters have been actually evaluated for each wavefront reconstruction: the peak to valley (PV) and the rms. The PV is smaller at medium temperatures, where the wavefront is neither astigmatic nor spherical. Nevertheless at the operational set points the PV is always <0.6 λ .

Alternatively, Fig. 14 shows the change of the measured rms at each step along cycle 1 and 4. The maximum WFE(rms) is 0.14 λ (or ~88 nm at 633 nm wavelength). These measurements are well below our requirements and show a good repeatability. The bottom plot shows the nominal thermal conditions for each measurement.

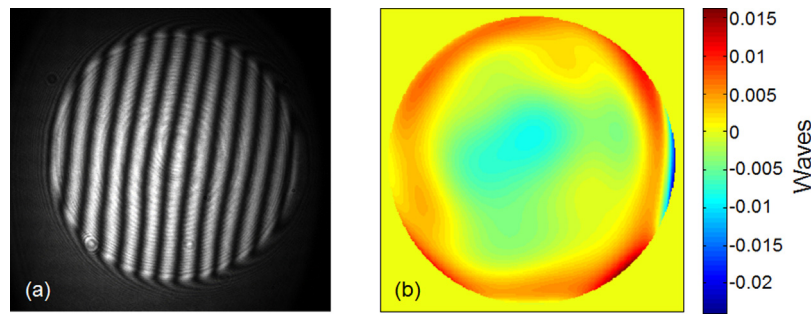


Fig. 9. The wavefront measurement method is based on a phase shifting interferometry technique that allows for inspection of the complete PMP optical aperture. (a) Interference fringe pattern produced by the optical setup. (b) Transmitted wavefront reconstruction obtained from an empty TVC at vacuum conditions (rms of 0.005λ and peak to valley $\lambda/25$).

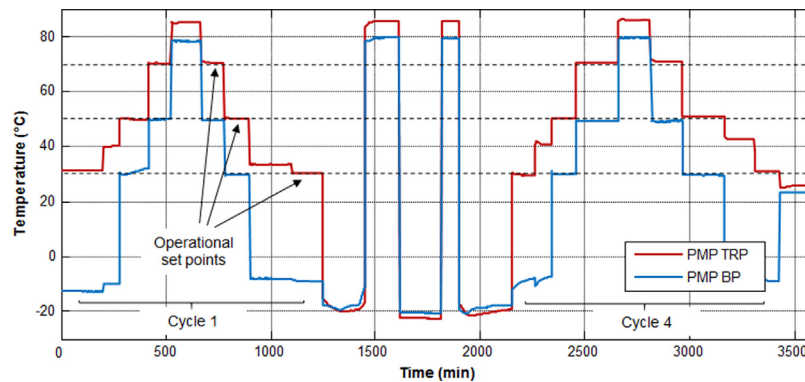


Fig. 10. Thermal cycles performed to the PMP at vacuum conditions.

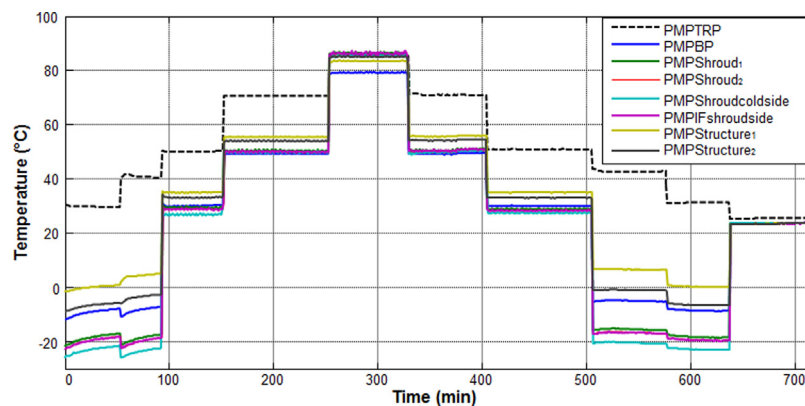


Fig. 11. Detail of the thermal readings obtained during the fourth cycle.

6.2. Optical retardance homogeneity

Within the PMP, birefringence and cell deformation can be thermo mechanically induced. The first, in particular, is a key parameter for our polarimetric requirements. Indeed, stress-induced birefringence can be simply produced by uneven clamping of the optical mountings [21]. Therefore the homogeneity of retardance, at the operational temperatures and across the clear aperture of the device, was also evaluated during the thermo-vacuum test. To do that the set up shown in Fig. 8 was partially used again. This time, however, the reference path was blocked, so that no fringes were formed at the detector. A white diffuse light source was used, instead of a laser, and a polarizer was placed before and after the TVC. The retardance homogeneity was then evaluated by taking images of the PMP under crossed polarizers.

Using this configuration, a set of images was obtained at each operational step during the thermal vacuum tests. The effective birefringence of the cell can be changed by application of a voltage, which induces different optical retardances in the orthogonal polarization components. The optical retardance introduced by each LCVR can be selected from the full 2π range for voltages with amplitudes lower than 14 V. A four-steps excitation signal was used during the tests and the last surface of the PMP is imaged by a color camera. A typical set of images captured is shown in Fig. 15. This basic go/no-go test can reveal many issues, such as a bad cavity sealing or irregular glue and LC molecules mixture next to the stopper. Stress induced birefringence can also be exposed with isochromatics. We have chosen to plot the worst case situation, in which the highest gradient between the PMP and its baseplate is set (sep-point 1). Nevertheless, in all the cases the images show a good

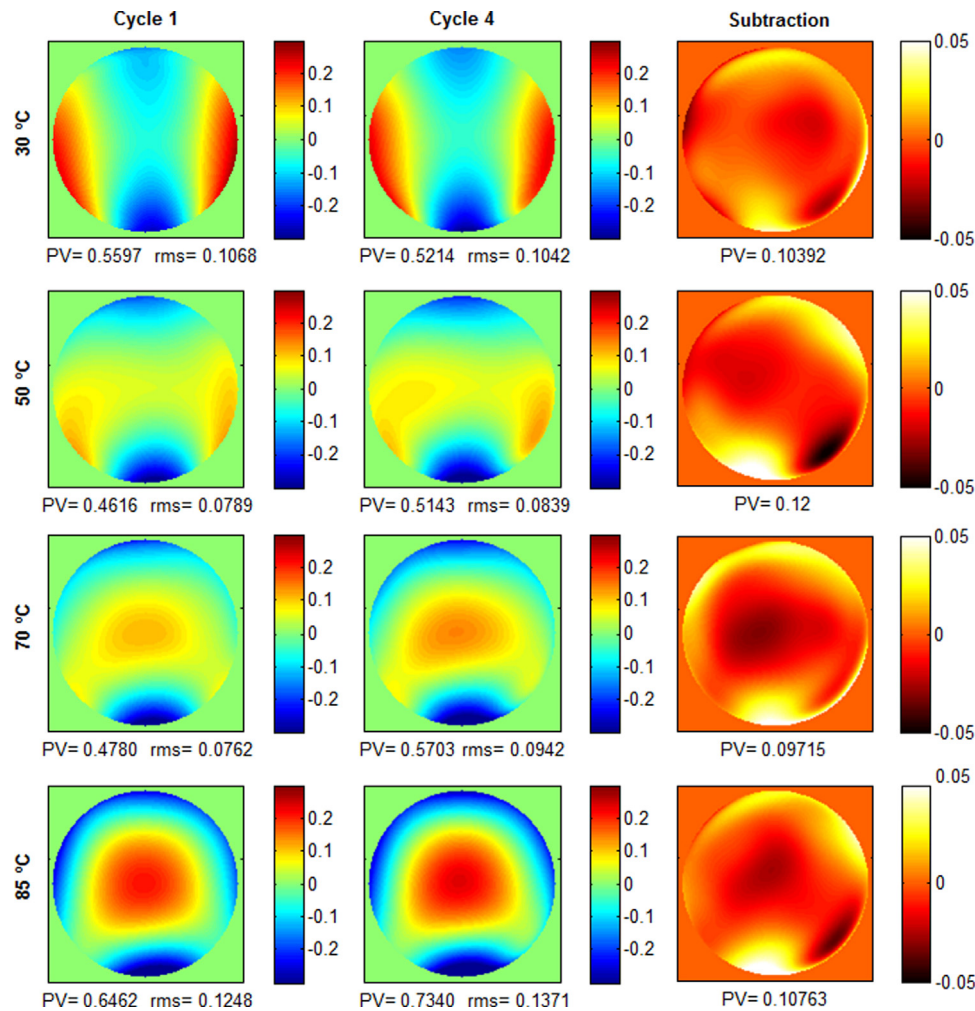


Fig. 12. PMP transmitted wavefront reconstruction in vacuum conditions at the science set-points (in waves). The fourth row also shows the results at the maximum operational temperature of 85 °C. The first and second column correspond to measurements performed during the first and fourth cycle respectively. The wavefront map covers the whole PMP clear aperture (30 mm diameter). The filling inlet of the cell is at the bottom of the images. As the temperature is increased the wavefront aberration evolution, from astigmatic to spherical, is apparent. The third column shows the subtraction of both wavefronts, showing a nearly flat residual (notice the change in scale).

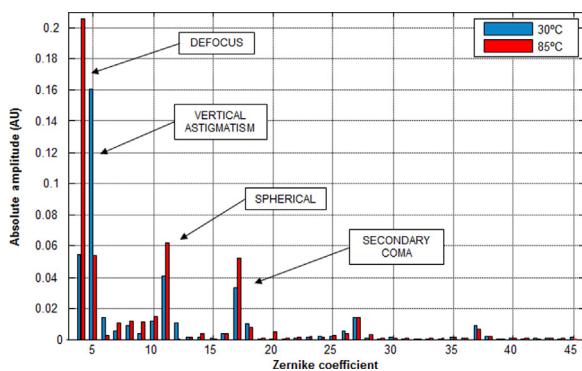


Fig. 13. Zernike coefficient decomposition of two wavefront measurements performed at different temperatures. Piston and tilt coefficients have been omitted for clarity.

homogeneity across the clear aperture, and no features were seen during the tests at any temperature condition.

6.3. Discussion

A thermo-vacuum cycling test, which is part of the acceptance campaign of the PMP flight model, was carried out. It consists of

four thermal cycles performed at acceptance levels. The thermal control set the expected environmental conditions and the PMP set-points defined. It also met the required stability. In addition optical quality and retardance homogeneity measurements were performed at the PMP operational set-points. Extra measurements were obtained at room temperature and at 85 °C. The WFE shows an astigmatic aberration at 30 °C with increasing defocus at 50 °C and 70 °C, with a repetitive behavior in each cycle. The PV was maximum at the lower temperature and always $<0.6\lambda$. The rms was evaluated to be within requirements (<88 nm) showing a similar trend from cycle to cycle. Alternatively, the PMP retardance homogeneity, measured during the thermal cycling test, was performed with the LCVR driving voltage activated. The optical clear aperture images showed a good homogeneity under crossed polarizers at each step of the thermal cycle test, thus verifying the LCVR functionality.

7. Performance at non-operational temperature ranges

The PMP performance has been also characterized after being subjected to a thermal cycle at the mission non-operational temperatures. As shown in Table 1, this temperature range goes from -40 °C to 90 °C and it includes the qualification margin levels. The thermal cycle was done under vacuum conditions lower than

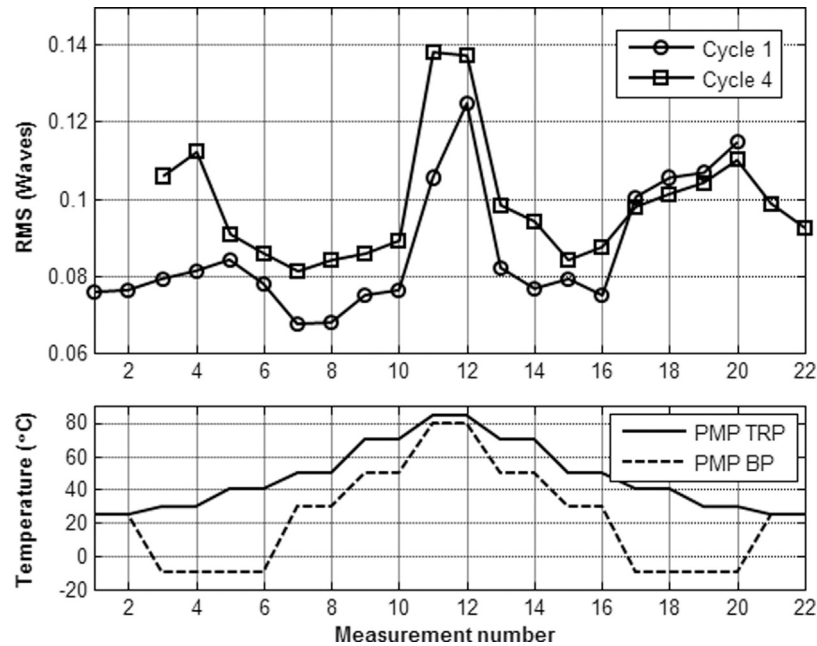


Fig. 14. RMS obtained from cycle 1 and 4. The horizontal axis corresponds to the wavefront transmitted measurement performed. The bottom plot corresponds to the thermal conditions at each cycle and measurement. Two measurements were performed at each step.

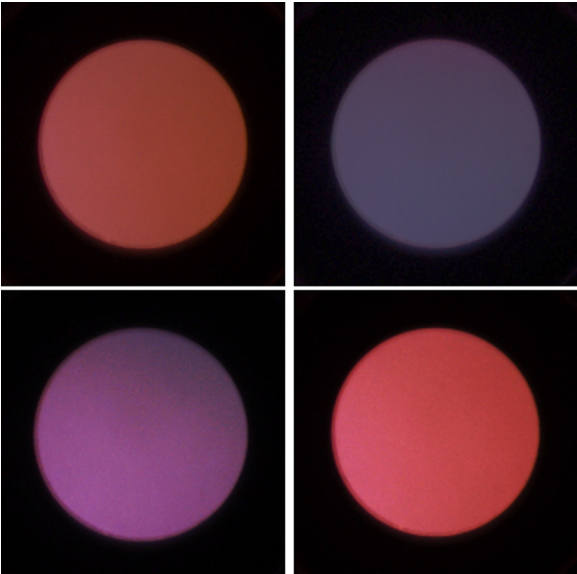


Fig. 15. PMP clear aperture through crossed polarizers at 30 °C. Each color corresponds to a different optical retardance electrically induced.

0.1 mPa. The dwell time in the maximum and minimum temperatures was 2 h, the stabilization criteria in those temperatures was 1 °C/h and the temperature slope during the transition phases was lower than 3 °C/min.

The PMP optical features evaluated were the transmitted wavefront error, the beam deviation and the polarimetric modulation efficiencies at 40.0 ± 0.5 °C. These parameters are listed, before and after a thermal cycle at non-operational temperatures, in Table 5.

This time, the transmitted WFE measurement was performed using a commercial Fizeau-type interferometer. Since the measurements could be done outside the TVC, we used the interferometer (DynaFiz model, Zygo) to evaluate the PMP clear aperture (30 mmØ). The values found were within the ranges previously measured during the thermo-vacuum cycle campaign. Alterna-

Table 5
PMP performances before and after a thermal cycle at non-operational temperatures. The polarimetric modulation efficiencies (ϵ_2 , ϵ_3) evaluated are also listed.

	Before	After	Requirement
WFE (rms)	46 nm	51 nm	<100 nm
Beam deviation	<5 arcsec	<5 arcsec	<5arcmin
ϵ_2	0.67 ± 0.01	0.66 ± 0.01	>0.6
ϵ_3	0.682 ± 0.009	0.680 ± 0.007	>0.6

tively, the beam deviation produced by the PMP was determined using two opposed autocollimators (Trioptics and Nikon).

Finally, a fixed polarizer and a rotating quarter waveplate was arranged to set a polarization state generator. This system was used to measure the PMP polarimetric modulation efficiencies within a ±2° field of view in a collimated beam configuration.

The polarimetric efficiencies are defined in Ref. [22] and a detailed explanation is out of the scope of this work. They are, however, critical parameters for the PMP performance. For METIS, only the efficiencies associated to the linear polarization components of the Stokes vector, Q and U (ϵ_2 and ϵ_3 respectively) are of interest. Overall, these parameters were all found to be within the values required, and the PMP did not show any performance degradation when the unit returned to the room conditions. The polarimetric calibration methodology and the experimental results will be described in depth in an upcoming publication.

8. Conclusions

The PMP is a key subsystem for the METIS coronagraph, an instrument on board the SoLo mission. In this paper the PMP flight model, a LCVR based polarimeter modulator, was described. Some of its most critical requirements are dictated by the thermal conditions expected during the mission and the thermal stability required to obtain reliable measurements. Thus a thermal simulation of the PMP and the test setup was run to model a representative thermal environment. This analysis demonstrated that the conditions can be met by our experimental arrangement.

Then, a thermal cycling test, which is part of the acceptance campaign, was carried out. It consists of four thermal cycles

performed at acceptance level. During these thermal cycles the transmitted WFE (PV and rms) was evaluated by means of a dedicated phase shifting interferometer. This test has shown that the WFE has an elastic and repetitive behavior along the thermal cycles and that the aberrations induced were within the optical requirements. Also it was demonstrated that the planned temperature set-points can be achieved with the power budget available for the active thermal control. At the same time, the LCVRs were electrically driven and the retardance homogeneity was monitored across the clear aperture of the device, showing a good homogeneity. Other optical tests were performed at the non-operational conditions and they revealed no device degradation.

As a consequence, it has been demonstrated that the PMP flight model meets the requirements specified, and that it is sufficiently robust against the thermal environment expected for the space mission.

Acknowledgments

The authors would like to express their gratitude to the rest of the INTA and METIS teams for their scientific and technical support. Additionally the authors gratefully acknowledge the financial support provided to this research by the MINECO (Ministerio de Economía Industria y Competitividad, Gobierno de España), project ESP2014-56169-C6-3-R “Fabricación e integración de los modelos QM, FM y FS de SO/PHI (Polarimetric and Helioseismic Imager for Solar Orbiter)” and by the Agenzia Spaziale Italiana (ASI).

References

- [1] D. Müller, R.G. Marsden, O.C.S. Cyr, H.R. Gilbert, Solar Orbiter exploring the Sun-heliosphere connection, *Solar Phys.* 285 (2013) 25–70, <http://dx.doi.org/10.1007/s11207-012-0085-7>.
- [2] S. Fineschi, E. Antonucci, M. Romoli, A. Bemporad, G. Capobianco, et al., Nobel Space Coronagraph: METIS, a flexible design for multi-wavelength imaging and spectroscopy, in: S. Fineschi, J. Fennelly (Eds.), *Solar Physics and Space Weather Instrumentation V*, Proc. of SPIE, vol. 8862, 2013, <http://dx.doi.org/10.1117/12.2028544>.
- [3] G. Crescenzo, S. Fineschi, G. Capobianco, G. Nicolini, G. Massone, M.A. Malvezzi, F. Landini, M. Romoli, E. Antonucci, Imaging polarimetry with the METIS coronagraph of the Solar Orbiter mission, in: T. Takahashi, S.S. Murray, J.A. den Herder (Eds.), *Space Telescopes and Instrumentation*, Proc. of SPIE, vol. 8443, 2012, <http://dx.doi.org/10.1117/12.927432>.
- [4] R.L. Heredero, N. Uribe-Patarroyo, T. Belenguer, G. Ramos, A. Sánchez, M. Reina, V.M. Pillet, A. Álvarez-Herrero, Liquid-crystal variable retarders for aerospace polarimetry applications, *Appl. Opt.* 46 (2007) 689–699, <http://dx.doi.org/10.1364/AO.46.000689>.
- [5] A. Álvarez-Herrero, N. Uribe-Patarroyo, P. García-Parejo, J. Vargas, R.L. Heredero, R. Restrepo, V. Martínez-Pillet, J.C. del Toro-Iniesta, A. López, S. Fineschi, G. Capobianco, M. Georges, M. López, G. Boer, I. Manolis, Imaging polarimeters based on liquid crystal variable retarders: an emergent technology for space instrumentation, in: J.A. Shaw, J.S. Tyo (Eds.), *Polarization Science and Remote Sensing V*, Proc. of SPIE, vol. 8160, 2011, <http://dx.doi.org/10.1117/12.892732>.
- [6] V. Martínez-Pillet, J.C. del Toro-Iniesta, A. Álvarez-Herrero, et al., The Imaging Magnetograph eXperiment (IMaX) for the Sunrise balloon borne solar observatory, *Solar Phys.* 268 (2011) 57–102, <http://dx.doi.org/10.1007/s11207-010-9644-y>.
- [7] K. Solanki, T.L. Riethmüller, P. Barthol, S. Danilovic, W. Deutsch, H.P. Doerr, A. Feller, A. Gandorfer, D. Germerott, L. Gizon, B. Grauf, K. Heerlein, J. Hirzberger, M. Kolleck, A. Lagg, R. Meller, G. Tomasch, M. van Noort, J.B. Rodríguez, J.L.G. Blesa, M.B. Jiménez, J.C.D.T. Iniesta, A.C.L. Jiménez, D.O. Suárez, T. Berkefeld, C. Halbgewachs, W. Schmidt, A. Álvarez-Herrero, L. Sabau-Graziati, I.P. Grande, V.M. Pillet, G. Card, R. Centeno, M. Knölker, A. Lecinski, The second flight of the SUNRISE balloon-borne solar observatory: overview of instrument updates, the flight, the data and first results, *Astrophys. J. Suppl. Ser.* 229 (2017) 2, <http://dx.doi.org/10.3847/1538-4365/229/1/2>.
- [8] A. Álvarez-Herrero, P. García-Parejo, H. Laguna, J. Villanueva, J. Barandiarán, L. Bastide, M. Reina, A. Sánchez, A. Gonzalo, R. Navarro, I. Vera, M. Royo, Polarization modulators based on liquid crystal variable retarders for the Solar Orbiter mission, in: J.A. Shaw, D.A. LeMaster (Eds.), *Polarization Science and Remote Sensing VII*, Proc. of SPIE, vol. 9613, 2015, <http://dx.doi.org/10.1117/12.2188591>.
- [9] A. Gandorfer, S.K. Solanki, J. Woch, V. Martínez-Pillet, A. Álvarez-Herrero, T. Appourchaux, The Solar Orbiter mission and its Polarimetric and Helioseismic Imager, *J. Phys. Conf. Ser.* 271 (2011) 012086, <http://dx.doi.org/10.1088/1742-6596/271/1/012086>.
- [10] R. Roelfsema, H.M. Schmid, J. Pragt, et al., The ZIMPOL high-contrast imaging polarimeter for SPHERE: design, manufacturing, and testing, in: I.S. McLean, S.K. Ramsay, H. Takami (Eds.), *Ground-Based and Airborne Instrumentation for Astronomy III*, Proc. of SPIE, vol. 7735, 2010, <http://dx.doi.org/10.1117/12.857045>.
- [11] L. Kolokolova, J. Hough, A. Levasseur-Regourd, *Polarimetry of Stars and Planetary Systems*, Cambridge University Press, 2015, <http://dx.doi.org/10.1017/CBO9781107358249>.
- [12] P. Scherrer, J. Schou, R. Bush, A. Kosovichev, R.S. Bogart, J.T. Hoeksema, Y. Liu, T.L. Duvall, J. Zhao, A.M. Title, C.J. Schrijver, T.D. Tarbell, S. Tomczyk, The Helioseismic and Magnetic Imager (HMI) investigation for the Solar Dynamics Observatory (SDO), *Solar Phys.* 275 (2012) 207–227, <http://dx.doi.org/10.1007/s11207-011-9834-2>.
- [13] N. Uribe-Patarroyo, A. Álvarez-Herrero, V. Martínez-Pillet, Preflight calibration of the Imaging Magnetograph eXperiment polarization modulation package based on liquid-crystal variable retarders, *Appl. Opt.* 51 (2012) 4954–4970, <http://dx.doi.org/10.1364/AO.51.004954>.
- [14] F. Landini, M. Romoli, G. Capobianco, S. Vives, S. Fineschi, G. Massone, D. Loreggia, E. Turchi, C. Guillon, C. Escolle, M. Pancrazzi, M. Focardi, Improved stray light suppression performance for the Solar Orbiter/METIS inverted external occulter, in: S. Fineschi, J. Fennelly (Eds.), *Solar Physics and Space Weather Instrumentation V*, Proc. of SPIE, vol. 8862, 2013, <http://dx.doi.org/10.1117/12.2024209>.
- [15] M. Bass, *Handbook of Optics*, vol. II, 2nd ed., McGraw Hill Inc., 1995.
- [16] E. C. for Space Standardization, *Space product assurance. Black-anodizing of metals with inorganic dyes*, ECSS Q-ST-70-03C, ESA Requirements and Standards Division, Noordwijk, The Netherlands, 2008.
- [17] N. Uribe-Patarroyo, A. Álvarez-Herrero, P. García-Parejo, J. Vargas, R.L. Heredero, R. Restrepo, V.M. Pillet, J.C. del Toro Iniesta, A. López, S. Fineschi, G. Capobianco, M. Georges, M. López, G. Boer, I. Manolis, Space-qualified liquid-crystal variable retarders for wide-field-of-view coronagraphs, in: S. Fineschi, J. Fennelly (Eds.), *Solar Physics and Space Weather Instrumentation IV*, Proc. of SPIE, vol. 8148, 2011, <http://dx.doi.org/10.1117/12.904919>.
- [18] Z. Wang, B. Han, Advanced iterative algorithm for phase extraction of randomly phase-shifted interferograms, *Opt. Lett.* 29 (2004) 1671–1673, <http://dx.doi.org/10.1364/OL.29.001671>.
- [19] J. Vargas, N. Uribe-Patarroyo, J.A. Quiroga, A. Álvarez-Herrero, T. Belenguer, Optical inspection of liquid crystal variable retarder inhomogeneities, *Appl. Opt.* 49 (2010) 568–574, <http://dx.doi.org/10.1364/AO.49.000568>.
- [20] J.M. Bioucas-Dias, G. Valadão, Phase unwrapping via graph cuts, *IEEE Trans. Image Process.* 16 (2007) 698–709, <http://dx.doi.org/10.1109/TIP.2006.888351>.
- [21] P.R. Yoder, *Opto-Mechanical System Design*, 2nd ed., Marcel Dekker Inc., 1993.
- [22] J.C. del Toro Iniesta, M. Collados, Optimum modulation and demodulation matrices for solar polarimetry, *Appl. Opt.* 39 (2000) 1637–1642, <http://dx.doi.org/10.1364/AO.39.001637>.

Biographies

Manuel Silva-López graduated in Physics at the Sevilla University in Spain in 2002. He then moved to Edinburgh, United Kingdom, where he obtained his Ph.D. in optics in 2007 at Heriot-Watt University. After a period working as researcher at different universities, he joined the National Institute of Aerospace Technology (INTA) at Madrid, Spain, in 2013. At INTA he is working in the development of optical based instrumentation for space.

Laurent Bastide graduated in 2006 as an Aerospace Engineer at the IPSA School in Paris. He has then several experiences in companies of the European space sector such as Thales Alenia Space and Airbus Defence and Space before joining INTA in 2009 as a thermal engineer to design space payloads for scientific missions.

René Restrepo is a Mechanical Engineer at EAFIT University, Medellín, Colombia, DEA (MSc) in Physics and Computer Science at the University of La Laguna (ULL), Tenerife, Canary Islands – Spain. Ph.D. in Physics at the Complutense University of Madrid (UCM), Spain. He was a researcher at INTA and worked as an engineer at the Instituto de Astrofísica de Canarias (IAC) and at the Gran Telescopio de Canarias, Tenerife, Canary Islands – Spain. Currently, he is the Head of Applied Optics Group at EAFIT University.

Pilar García Parejo graduated in Chemistry at the Universidad Autónoma de Madrid (UAM), Spain, in 2003. She was awarded with the Ph.D. from the UAM, researching on the preparation and characterization of sol-gel coatings for optical applications. Currently, she works in the space instrumentation area of INTA, Madrid. Her research interests are focused on the development and characterization of materials and optical devices to be used in payloads for space missions.

Alberto Álvarez-Herrero received the degree in fundamental physics and the Ph.D. from the Complutense University of Madrid (UCM), Spain in 1994 and 2002, respectively. He has been at INTA since 1994 working in the development of space optical instrumentation. His research is aimed at new technologies, techniques, materials and devices to be used in payloads for space missions. Ellipsometry and polarimetry are his main areas of expertise. Currently he is focused on liquid crystal devices, nanostructured coatings and effects of the space environment on the optical properties of materials.